Chapter 5

Impedance and Beam Instabilities

This chapter focuses on the beam instabilities due to single-beam collective effects, impedance contributions from various beamline elements, ion trapping, and other issues in KEKB. We also discuss the power deposition generated by a beam in the form of the higher order mode (HOM) losses by interacting with its surroundings.

The dominant issues at KEKB in terms of beam instabilities are the very high beam current (2.6 A in the LER and 1.1 A in the HER) to achieve the high luminosity goal of $10^{34}\mathrm{cm}^{-2}\mathrm{s}^{-1}$, and a short bunch length (σ_z =4 mm) to avoid degradation of the luminosity by the hour-glass effect and a finite angle crossing. However, since the charges are distributed over many (up to 5120) bunches, the bunch current is not unusually high. As a consequence, single-bunch effects are expected to be relatively moderate; they are well below the stability limits with comfortable margins. The main concern, in turn, is coupled-bunch instabilities due to high-Q resonant structures such as RF cavities and the transverse resistive-wall instability at very low frequency (lower than the revolution frequency). The short bunch can pick up impedance at a very high frequency ($f \sim 20$ GHz), which can lead to an enormous heat deposition by the HOM. The deposited power is likely to be localized at places where wake fields can be trapped by small discontinuities in the beam chamber such as BPMs, or in regions partitioned by two objects inserted inside the beam chamber, such as masks at the interaction region (IR). This heating problem requires serious efforts to (i) reduce the impedance of various beam components or (ii) eliminate structures in the vacuum system which can trap higher order modes.

Other classes of issues include multi-bunch instabilities that may be caused by the effects of ionized gas molecules and photo-electrons in the ring. Some theoretical investigations have been made. They are also discussed in this chapter.

5.1 Impedance

In this section, we summarize our estimate of impedance contributions from various beamline components. Most of them are small discontinuities in the vacuum chamber wall which produce inductive impedance. Their wake potentials are almost a derivative of the delta-function, and therefore, their loss factors are mostly negligible. Among the impedance-generating elements in the rings, the largest contributors are RF cavities, the resistive wall, the IR chamber (including two recombination chambers at both ends), bellows (because of their large numbers), and their protection masks in the arc sections. The impedance of normal-conducting ARES and superconducting cavities will be described in detail in Chapter 8. We only show their loss factors at a bunch length σ_z of 4 mm for later use in the loss factor budget.

5.1.1 ARES RF cavities

When the ARES system is implemented at KEKB, the number of ARES cavities required is 20 for the LER and 40 for the HER. These numbers have been derived to compensate for the synchrotron radiation and HOM power losses, as well as to satisfy the requirement for the short bunch length. Using the program ABCI [1], we have estimated that the main body of the ARES cavity produces a loss factor of 0.529 V/pC for a bunch length of 4 mm. If this cavity is connected to the beam chamber (diameter=100 mm) at both ends with 100 mm long tapers,[1] the additional loss factor will be 0.363 V/pC [2]. In total, the loss factor of one cell of the ARES cavity is 0.892 V/pC.

5.1.2 Resistive-Wall

The material of the KEKB beam chamber was chosen to be copper because of its low photon-induced gas desorption coefficient, its high thermal conductivity, and its large photon absorption coefficient. Its high electrical conductivity also helps to reduce the resistive-wall impedance. Nevertheless, this is still the dominant source of transverse impedance for the coupled-bunch instability. The total transverse resistive-wall impedance of the circular pipe with an inner radius b is given by

$$Z_{RW}(\omega) = Z_0(\mathrm{sgn}(\omega) - i)\frac{\delta R}{b^3}, \tag{5.1}$$

[1]There is a possibility of not using tapers (the vacuum chamber with a diameter of 145 mm may run all the way through the straight section). The quote loss factor quoted will then represent the worst-case scenario.

where Z_0 ($\cong 377\Omega$) is the characteristic impedance of the vacuum, δ the skin depth, R the average radius of the ring, and sgn(ω) the sign of ω. For the LER vacuum chamber ($b \cong 50$ mm), Eq. (5.1) gives the resistive-wall impedance of 0.3 MΩ/m at the revolution frequency 100 kHz, while the impedance decreases to 2 kΩ/m at the cutoff frequency 2.3 GHz of the chamber. The HER vacuum chamber, which has a racetrack cross section shape, may be approximated by a circular one with a radius of 25 mm.

5.1.3 Masks at Arc

Each bellows has a mask (5 mm high) located at its front side so that it is shielded from the synchrotron radiation from a nearby bending magnet. There are about 1000 bellows (one bellows on both sides of each quadrupole magnet. There will be no mask for the BPMs). The cross section of the mask in the medium plane is shown in Fig. 5.1.

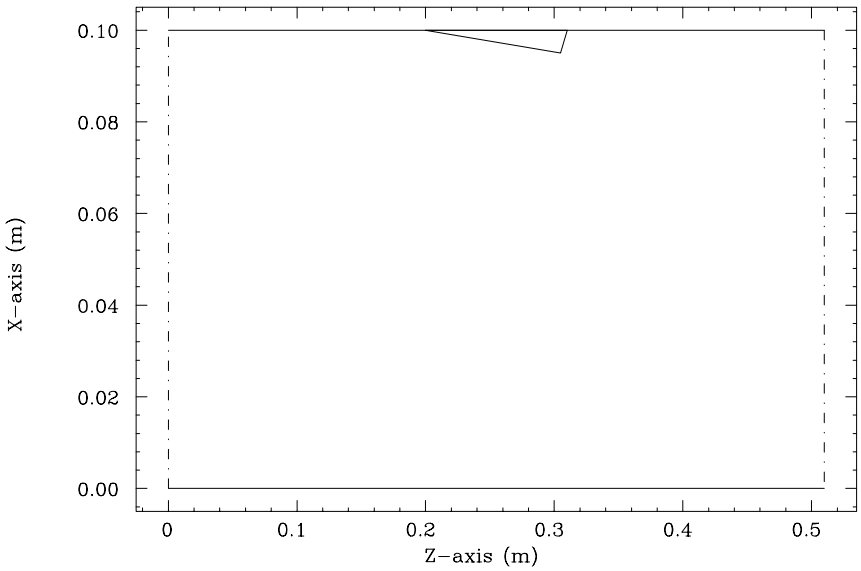

Figure 5.1: Mask at arc

For accurate calculations of the wake potentials and loss factors, a 3-D program called MASK30 has been developed to solve the Maxwell equations directly in the time domain. Using this code, we have found that the total longitudinal impedance of 1000 masks is

$$\mathrm{Im}[\frac{Z(\omega)}{n}] = 2.8 \times 10^{-3} \ \ \Omega, \tag{5.2}$$

where n expresses the frequency ω divided by the revolution frequency ω_0, $n = \omega/\omega_0$. The total loss factor is

$$k_{\mathrm{L}} = 4.6 \ \ \mathrm{V/pC}, \tag{5.3}$$

which corresponds to a total HOM power of 62 kW in the LER.

5.1.4 Pumping Slots

The current design of the pumping slots adopts a so-called "hidden holes" structure, which is similar to those of HERA and PEP-II. A slot has a rectangular shape with rounded edges, which is long in the beam-axis direction (100 mm long, 4 mm wide). The slot is patched on the pumping chamber side by a rectangular grid. They help to prevent microwave power generated somewhere else from penetrating through the slots to the pumping chamber, and then depositing the energy in the NEG pumps. Analytic formulae exist for calculating impedance and loss factor of such a narrow slot with length l and width w by Kurennoy and Chin[3]. The formula for the inductive impedance can be written at low frequency (until the wavelength becomes comparable to the slot width) as

$$\mathrm{Im}[Z(\omega)] \approx -0.1334\ Z_0 \frac{\omega}{c} \cdot \frac{w^3}{4\pi^2 b^2}, \tag{5.4}$$

where c is the speed of light. The thickness correction to the above formula was studied by Gluckstern[4]. It tends to reduce the impedance by 44% compared with that for the zero-thickness case. The total impedance of the pumping slots at arc (there are 10 slots per port and there are 1800 ports in total) with a thickness correction is

$$\mathrm{Im}[\frac{Z(\omega)}{n}] = 1.1 \times 10^{-3}\ \ \Omega. \tag{5.5}$$

The total loss factor was calculated to be

$$k_{\mathrm{L}} = 0.37\ \ \mathrm{V/pC}. \tag{5.6}$$

There will be additional contributions from pumping slots in the straight section. Among them, only those at the wiggler section have been designed. A rough estimate shows that they will increase the above values for the impedance and the loss factor by about 10%.

5.1.5 BPMs

The annular gap (or groove) in a BPM between the button electrode and the supporting beam chamber can be approximated by a regular octagon. The impedance of a BPM can thus be calculated with the same formula for a narrow slot, by considering it as a combination of eight narrow slots (two transverse, two longitudinal, and four tilted)[5]. If we neglect small contributions from the longitudinal slots, and consider four tilted

slots as two transverse ones, the impedance of the BPM becomes equivalent to that of the four transverse slots. For a transverse slot, equation (5.4) is replaced by

$$\mathrm{Im}[Z(\omega)] \approx -Z_0 \frac{\omega}{c} \frac{\alpha_m}{4\pi^2 b^2}, \tag{5.7}$$

where

$$\alpha_m = \frac{2}{3}(\frac{\pi}{4})^2 \frac{a^3}{\ln \frac{2\pi a}{w} + \frac{\pi t}{2w} - \frac{7}{3}} \tag{5.8}$$

is the longitudinal magnetic polarizability. The other parameters are: a, the radius of the annular gap; w , the width of the gap; and t, the thickness of the chamber wall. In our case, they are numerically, $a = 6.5$ mm, $w = 1$ mm, and $t = 1$ mm. For 400 four-button BPMs, the total inductive impedance is

$$\mathrm{Im}[\frac{Z(\omega)}{n}] = 1.3 \times 10^{-4} \ \ \Omega. \tag{5.9}$$

The total loss factor of the BPMs has been computed using the T3 code of MAFIA, and found to be

$$k_{\mathrm{L}} = 0.79 \ \ \mathrm{V/pC}. \tag{5.10}$$

There is a theory [6] which predicts that small holes or slots in the beam chamber can create localized trapped modes in their vicinity. These trapped modes can give rise to sharply peaked behavior of the impedance slightly below the cutoff frequencies of the corresponding propagating modes in the beam chamber. These narrow resonances may drive coupled-bunch instabilities. We have estimated the shunt impedance and the Q-value of such a trapped mode created by the gap in the BPM at the first cutoff frequency of the LER chamber (2.3 GHz) according to Kurennoy-Stupakov's formulae. In this calculation, we assumed that the radiated fields through the gap in the outer space (=inside the BPM) will propagate away freely, and will not resonate in the BPM. Our BPMs have been designed to satisfy this condition. The resulting shunt impedance is

$$R = 1.56 \times 10^{-6} \ \ \Omega \tag{5.11}$$

per one button of the BPM. The Q-value is 0.7×10^5, and the resonant frequency is only by 1.8 Hz below the cutoff frequency. Thus, this mode is likely to propagate away quickly by coupling with the TM mode of the beam chamber. Besides, the shunt impedance given by (5.11) is completely negligible compared with those of HOMs in the cavity.

5.1.6 Mask at IP

There are four masks (two large and two small) on both sides of the beryllium chamber at the interaction point (IP) to shield it from direct synchrotron radiation. Figure 5.2 shows their geometry.

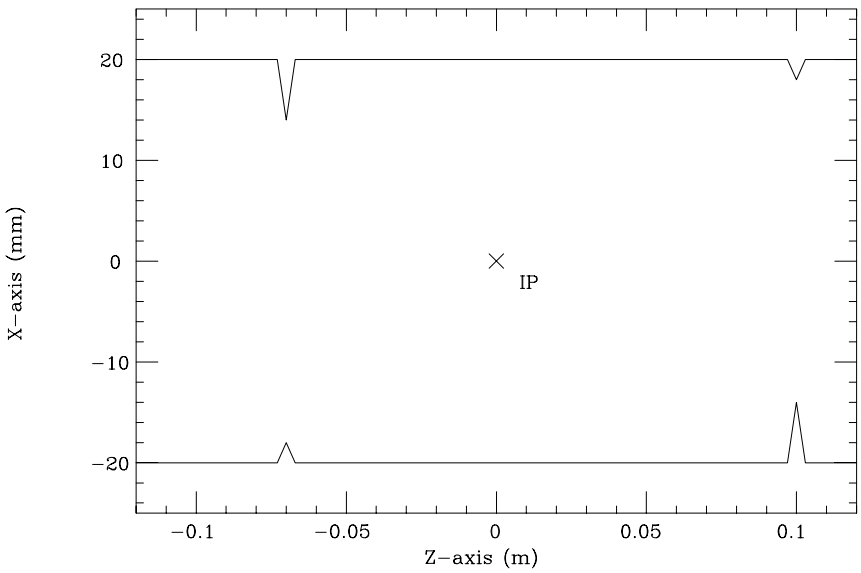

Figure 5.2: Mask at the IP.

The loss factor due to these masks has been calculated using the code MASK30, and was found to be

$$k_{\mathrm{L}} = 0.08 \ \ \mathrm{V/pC}. \tag{5.12}$$

This value is about one-fourth that obtained by ABCI using the axially symmetrical model. The ratio of the two loss factors agrees with the ratio of the opening angle of the IP mask from the beam axis (about 90 degrees) to that of an entire circle. It is seen that a rough estimate of the loss factor can be obtained by multiplying the result for an axially-symmetric model by a factor that corresponds to the solid angle covered by the asymmetric model of interest.

Not all of the power generated at the IP will be deposited there. This depends on the Q-values of modes excited between the masks. The beam chamber at the IP has a cutoff frequency at 6.36 GHz, and the tips of the taller masks create another cutoff frequency at 8.20 GHz. It was estimated using the MASK30 code that if the wake fields between these two frequencies are trapped, the deposited power by two (an electron and a positron) bunches at the IP will be

$$\mathrm{P} = 0.0084 \ \mathrm{V/pC} \times (2.6 + 1.1) \ \mathrm{A} \times (5.23 + 2.22) \ \mathrm{nC} = 240 \ \ \mathrm{W}, \tag{5.13}$$

which is 20% more than the design tolerance of 200 W for a beryllium chamber. However, a careful examination using an axially symmetric model for the IP masks showed that the actual Q-values of the modes between 6.36 - 8.20 GHz are at most 70, which is much smaller than Q $\sim 1.4 \times 10^4$ based on the finite conductivity of the beryllium chamber. This is because the radius of the beam chamber remains the same inside and outside of the IP region separated by the masks, and therefore, the modes can escape to the outside region by making a bridge over the masks. Consequently, less than 0.5%($= 70/(1.4 \times 10^4)$) of the HOM power created at the IP is deposited there (P$\leq$ 1.2W). Even if these modes are resonant with the bunch spacing causing a build-up of wake fields, the maximum enhancement factor for a mode on the resonance is only

$$\mathrm{D_{max}} = \frac{4Qc}{\omega_m s_b} \sim 3.5, \tag{5.14}$$

where ω_m is a typical mode frequency and s_b is the bunch spacing. Therefore, the maximum power deposition is $\mathrm{D_{max}}$P $\leq$ 4.2W. The actual 3-D masks at the IP have a more open structure than the axially symmetric model, and thus the power deposition might be even smaller.

A more serious problem may be a dissipation of the HOM power generated at other parts of the IR chamber, which propagates to the IP region. As will be seen in the next two subsections, a HOM power of about 26 kW will be created in the entire IR region. If the same factor (0.5%) found above can be used as the efficiency for the power deposition at the IP, we can estimate that a power of about 130 W will be deposited at the IP out of 26 kW.

5.1.7 IR Chamber

The vacuum chamber inside the experimental facility makes two large shallow tapers. Its layout is sketched in Fig. 5.3. Its impedance has been calculated using ABCI and was found to be mostly inductive,

$$\mathrm{Im}[\frac{Z(\omega)}{n}] = 1.0 \times 10^{-3} \ \ \Omega. \tag{5.15}$$

The loss factor without any contribution from the IP masks is

$$k_L = 0.29 \ \ \mathrm{V/pC}, \tag{5.16}$$

which corresponds to a HOM power loss of 4 kW. This power deposition as well as the power generated at the recombination chambers must be taken care of by e.g., putting an absorber in the chambers.

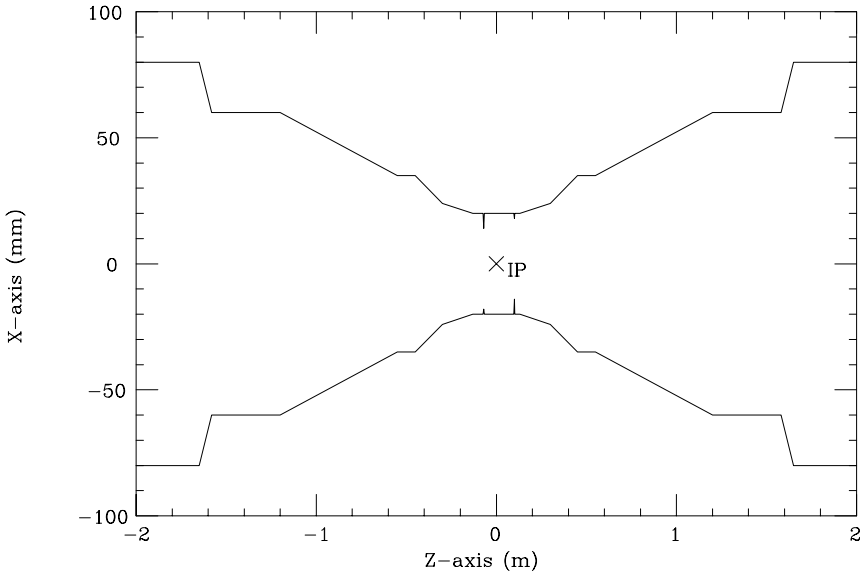

Figure 5.3: Layout of the IR chamber.

5.1.8 Y-shaped recombination chambers

The LER and HER chambers are combined to make a single chamber on both sides of the IP (about 3 m away). The impedance and loss factors of two recombination chambers were modeled as axially symmetric structures, and the results by ABCI were then averaged in proportion to the azimuthal filling factors. It is found to give a large loss factor, almost equivalent to that of two ARES cavities,

$$k_{\rm L} = 1.6 \ \ {\rm V/pC}, \tag{5.17}$$

which corresponds to a HOM power loss of 22 kW due to the low energy beam.

5.1.9 Bellows

As explained in the subsection for the masks at arc, there are about 1000 shielded bellows in both rings (one bellows on both sides of every quadrupole). We have adopted the so-called sliding-finger structure for bellows. Their layout in the LER is sketched in Fig. 5.4. The bellows in the HER have a similar structure. These bellows produce predominantly inductive impedance. Their impedance has been calculated using ABCI. The imaginary part of the total impedance and the total loss factor for 1000 bellows in the LER ring are

$$\mathrm{Im}[\frac{Z(\omega)}{n}] = 4.23 \times 10^{-3} \ \ \Omega \tag{5.18}$$

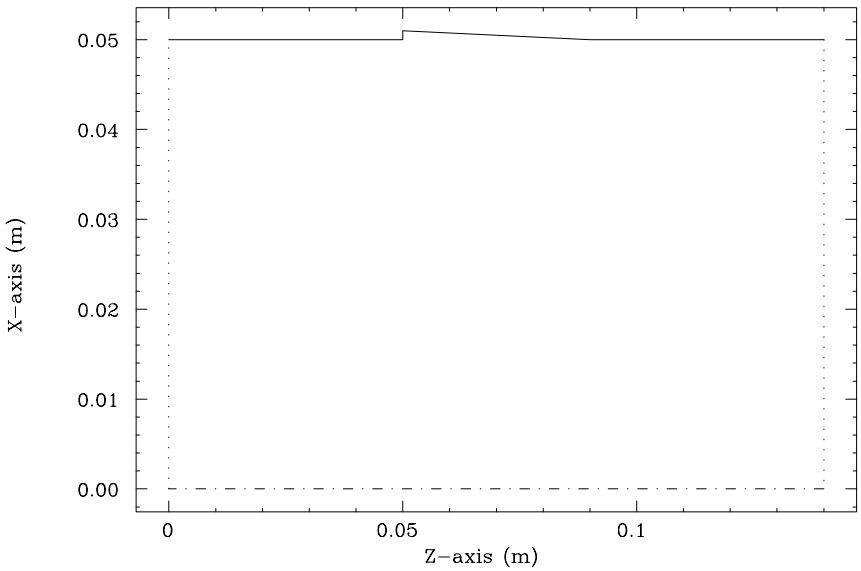

Figure 5.4: Bellows in the LER.

and

$$k_{\rm L} = 2.5 \ \ {\rm V/pC}. \tag{5.19}$$

They are $\mathrm{Im}[Z/n] = 0.8 \times 10^{-2}\ \Omega$ and $k_{\rm L} = 5.0$ V/pC in the HER.

Additional impedance is generated by the slits between the sliding fingers of the bellows. Using the same formula for a narrow slot, we found that their contributions are negligible.

5.1.10 Summary of Impedance Section

The inductive impedance and the loss factors of the individual elements in the LER are tabulated in Table 1.1. The total longitudinal wake potential for the LER is plotted in Fig. 5.5. The total HOM power deposition in the LER (corresponding to the loss factor of 32.1 V/pC) is P=440 kW. Without tapers for the ARES cavities, it is reduced to 330 kW. In the HER, the total inductive impedance would be comparable to that of the LER. The total loss factor in the HER is larger than that of the LER by 18 V/pC (10.6 V/pC without tapers) due to additional 20 RF cavities, leading to 50 V/pC (36.3 V/pC without tapers). The corresponding total HOM power deposition is 120 kW (90 kW without tapers). These numbers should be used in designing RF parameters.

Table 5.1: LER inductive impedance and HOM power loss budgets. The values in brackets are those without tapers for ARES cavities.

Component	Number of items	Inductive impedance Im[Z/n] (Ω)	Loss factor (V/pC)	HOM power (kW)
Cavities	20	—	17.8 (10.6)	243 (144)
Resistive-wall	3016 m	5.2×10^{-3} at 2.3 GHz	4.0	54
Masks at arc	1000	2.8×10^{-3}	4.6	62
Pumping slots	10×1800	1.1×10^{-3}	0.37	5.5
BPMs	4×400	1.3×10^{-4}	0.79	10.7
Mask at IP	1	negligible	0.08	1.1
IR chamber	1	1.0×10^{-3}	0.29	4
Recomb. chambers	2	-8.0×10^{-4}	1.6	22
Bellows	1000	4.23×10^{-3}	2.5	34
Total		0.015	32.1 (25.7)	440 (330)

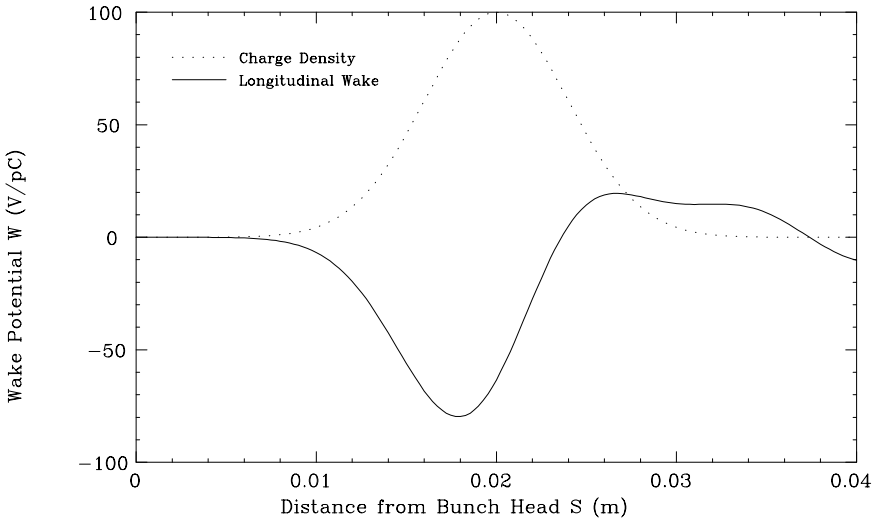

Figure 5.5: Total longitudinal wake potential for the KEKB LER.

5.2 Single-Bunch Collective Effects

In this section, we review our predictions of the singe-bunch collective effects, namely, the bunch lengthening and transverse mode-coupling instability. As mentioned earlier, these instabilities are expected to impose no fundamental limitation on the stored current, since the bunch current is relatively low compared to that of other large electron rings. However, the requirement of a short bunch ($\sigma_z = 4$ mm) demands that careful attention be paid to any possible causes for deviation from the nominal value. The transient ion problem and coupled-bunch instabilities due to photo-electrons will be discussed separately in sections 5.4 and 5.5, respectively.

5.2.1 Bunch Lengthening

There are two mechanisms to alter the bunch length from the nominal value. One is the potential-well distortion of the stationary bunch distribution due to the longitudinal wake potential. The deformed bunch distribution can be calculated by solving the Haissinski equation. The bunch can be either lengthened or shortened depending on the type of wake potential. Another mechanism is the microwave instability which has a clear threshold current for the onset of the instability.

Oide and Yokoya have developed a theory which includes both the potential-well distortion effect and the microwave instability [7]. A program is now available to compute the bunch length according to their theory. Figure 5.6 shows the calculated bunch length in the LER as a function of the number of particles in a bunch, N_p.

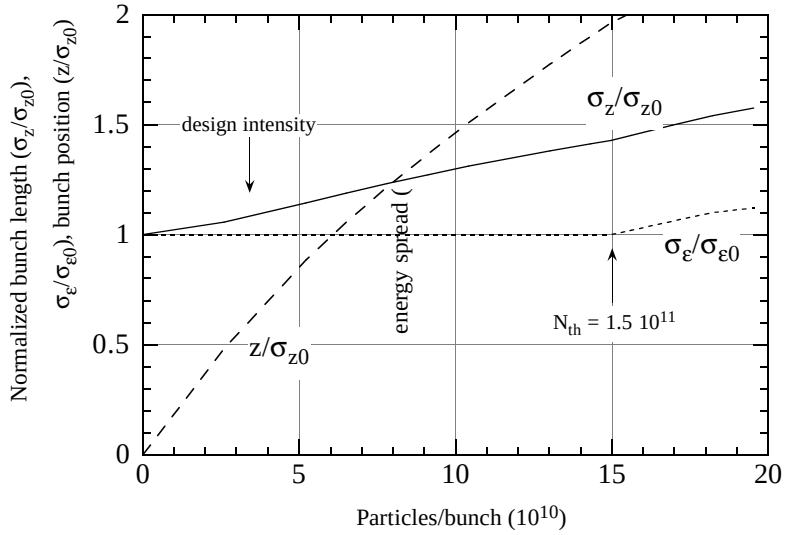

Figure 5.6: Bunch length and energy spread in the LER.

As can be seen, there is a constant bunch lengthening due to the potential-well distortion; and the microwave instability takes off at $N_p = 1.5 \times 10^{11}$, which is about four times larger than the proposed number of particles per bunch. At the design intensity, the bunch is lengthened by only 10%.

5.2.2 Transverse Mode-Coupling Instability

The transverse mode-coupling instability is known to be responsible for limiting the single-bunch current in large electron rings, such as PEP [8] and LEP. This instability takes place when two head-tail modes (m= 0 and m= -1 modes in most cases) share the same coherent frequencies. In the short bunch regime where the KEKB will be operated, the coherent frequency of the m= -1 mode keeps almost constant as a function of the bunch current, while that of the m= 0 mode keeps descending until it meets the m= -1 mode. Using the estimated transverse wake potential and the averaged beta function of 10 m, we found that the coherent tune shift of the m=0 dipole mode is only ~ -0.0002 at the design bunch current. This value is much smaller than the design value of the synchrotron tune (~ 0.017). Thus, the transverse mode-coupling instability will not impose a serious threat to the performance of KEKB.

5.3 Coupled-Bunch Instabilities

As mentioned earlier, the coupled-bunch instabilities due to high-Q structures, such as RF cavities and the resistive-wall beam pipes, are the main concerns in the KEKB rings because of the unusually large beam current. We have adopted the so-called damped-cavity-structure to sufficiently lower the Q-values of higher-order parasitic modes, typically less than 100. The calculation results of the longitudinal growth time due to the RF cavities will be given in detail in the RF section. Here, we focus on the transverse coupled-bunch instability due to the resistive-wall impedance and coupled-bunch instabilities (both transverse and longitudinal) that are excited by the crabbing mode of the crab cavity.

5.3.1 Transverse Resistive-Wall Instability

The growth rate of the instability in terms of the rigid particle model is given by

$$\tau_{RW}^{-1} = -\frac{\beta_\perp \omega_0 I_b}{4\pi E_b/e} \sum_{p=-\infty}^{\infty} \mathrm{Re}[Z_{RW}(\omega_{p,\mu,\nu_\beta})], \tag{5.20}$$

where

$$\omega_{p,\mu,\nu_\beta} = (pM + \mu + \nu_\beta)\omega_0. \tag{5.21}$$

Here, $\beta_\perp$ is the averaged beta function over the ring, $\mathrm{Re}[Z_{RW}]$ the real part of the resistive-wall impedance, I_b the beam current, E_b the beam energy, ν_β the betatron tune, μ the mode number of the coupled-bunch oscillation and M the number of bunches in the beam. In the above formula, it is assumed that the RF buckets are uniformly filled with equal numbers of particles (we ignore the effects of the gap in the bunch filling, which may be necessary to suppress ion trapping).

In Figures 5.7 and 5.8, the growth time of the most unstable mode in the LER and HER, respectively, are shown as a function of the betatron tune. In the current design of the LER (HER), the horizontal and vertical tunes are 45.52 (46.52) and 45.08 (46.08), respectively. The most unstable mode (5074 mode) in the LER has growth times of 5.9 and 8.1 msec at these tunes, respectively. On the other hand, the most unstable mode in the HER is the 5073 mode, which has growth times of 4.0 and 5.6 msec at the horizontal and vertical tunes, respectively. Conversely, plots of the growth time as a function of the coupled-bunch mode number at the tunes 45.52 and 46.52 for the LER and the HER are given in Figures 5.9 and 5.10, respectively.

One possible cure for this instability is a bunch-by-bunch feedback system. The growth rates obtained above are, however, close to the limit of the design capability of our feedback system. Fortunately, since the coherent frequencies of the unstable modes

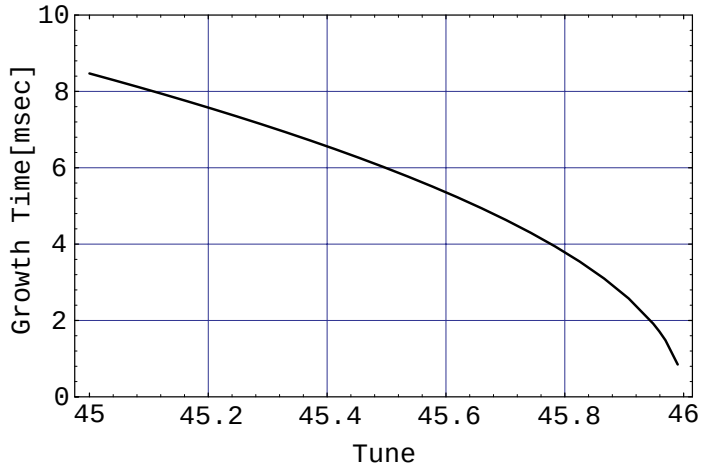

Figure 5.7: Growth time of the resistive-wall instability as a function of betatron tune in the LER.

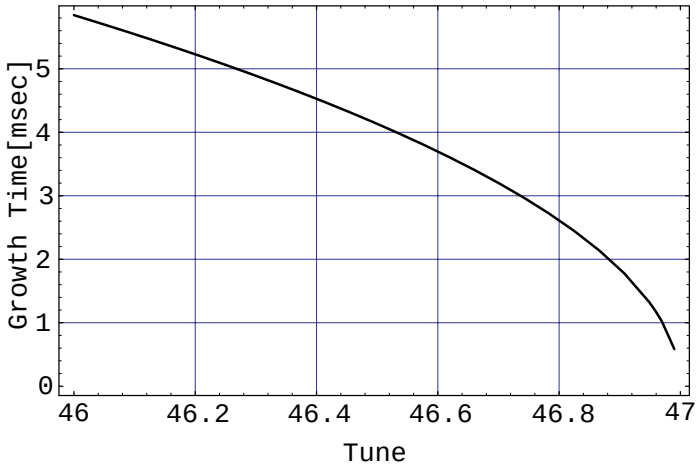

Figure 5.8: Growth time of the resistive-wall instability as a function of the betatron tune in the HER.

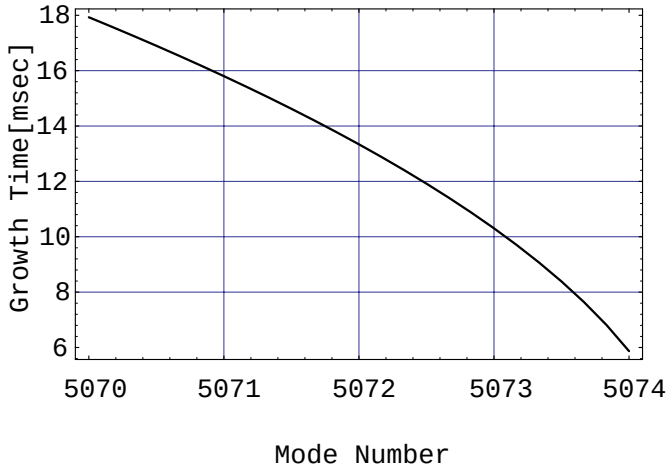

Figure 5.9: Growth time of the resistive-wall instability as a function of the mode number at the betatron tune of 45.52 in the LER.

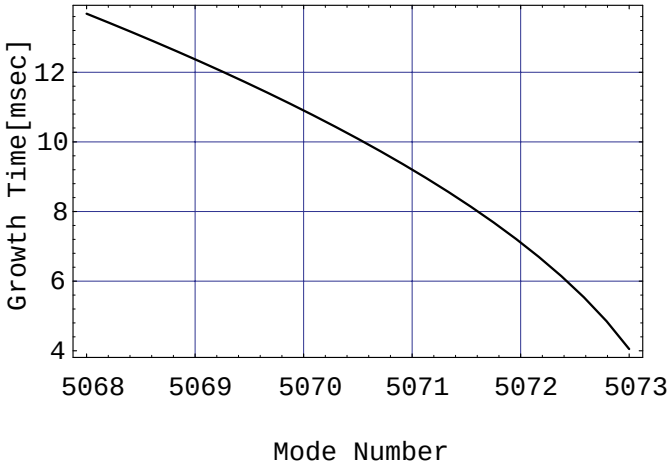

Figure 5.10: Growth time of the resistive-wall instability as a function of the mode number at the betatron tune of 46.52 in the HER.

stay in a narrow frequency range at low frequency, these modes may be stabilized by a narrow-band mode feedback system rather than a wide-band bunch-by-bunch feedback system. If the bunch-by-bunch feedback system can perform at a damping time of 10 msec, the mode feedback system must cover only one unstable mode for the LER and three modes for the HER, as seen from Figures 5.9 and 5.10. Then, a combination of two feedback systems is expected to provide a damping time of 1 msec for the fastest-growing modes.

5.3.2 Coupled-Bunch Instability by the Crabbing Mode

In this section we deal with only the instability due to the impedance of the crabbing mode. The instability due to the HOMs can be treated in a similar manner to those in accelerating cavities. The transverse coupling-impedance of a deflecting crabbing mode is expressed as

$$Z_\perp(\omega) = \frac{\omega_r}{\omega} \cdot \frac{\frac{R_\perp}{Q_0} Q_L}{1 + iQ_L(\frac{\omega}{\omega_r} - \frac{\omega_r}{\omega})}, \tag{5.22}$$

where ω_r is the resonant frequency of the crabbing mode, $R_\perp$ is the transverse shunt impedance, Q_0 is the unloaded Q-value and Q_L is the loaded Q-value. The most characteristic feature of the crabbing mode is that it operates at the same frequency as

Table 5.2: Main parameters of the crab cavity.

Beam energy	3.5 GeV
Beam current	2.6 A
Horizontal beta-function at the crab cavity	100 m
Horizontal betatron tune	45.52
Number of the crab cavities	2
Accelerating frequency	508.88 MHz
$R_\perp/Q_0$	277.4 Ω/m
Q_L	1×10^6

the accelerating mode unlike the HOMs. This feature renders this mode harmless by cancellation between the two betatron sidebands in both sides of the impedance peak, just like for the fundamental accelerating mode of a cavity. Unlike the accelerating mode, which must be detuned by a large amount of frequency to compensate for the heavy beam loading, we need not detune the crabbing mode. The growth rate of all coupled-bunch modes then almost vanishes as long as the resonant frequency of the crabbing mode is kept near the accelerating frequency.

The main parameters of the crab cavity, together with some machine parameters of LER, are summarized in Table 1.2.

The growth time of the most unstable mode (the 5074 mode for positive detuning, and the 5075 mode for negative detuning) in the LER is depicted in Fig. 5.11 as a function of the detuning frequency. In this figure, the radiation damping time (40 msec) with wiggler magnets is shown by the thick solid line. From this figure, it is clear that all modes are stable over a wide range of detuning from -6.5 kHz to 6.5 kHz. The growth time in the HER is even longer than in the LER. We can therefore conclude that the transverse coupled-bunch instability due to the crabbing mode will cause no serious problem as far as its frequency is well controlled.

Another problem may arise when the beam orbit has some offset at the cavity. In this case, longitudinal wake fields are excited which may cause a longitudinal coupled bunch instability. Even so, this type of instability can be stabilized by the fundamental mode of the accelerating cavities or by detuning the crab cavities to a lower frequency.

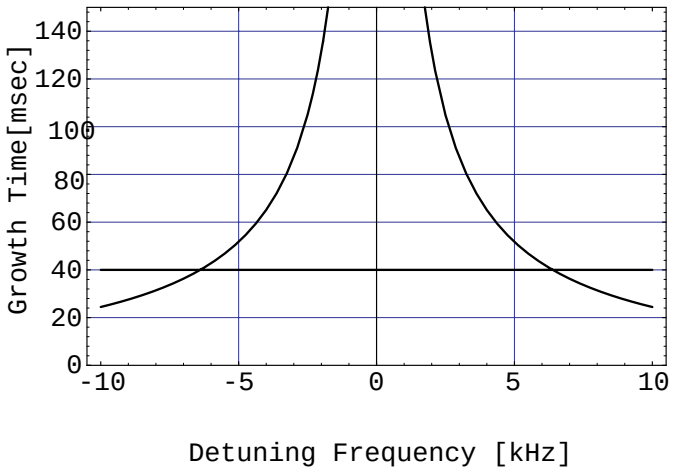

Figure 5.11: Growth time of the coupled bunch instability due to the crabbing mode in the LER versus the detuning frequency.

5.3.3 Summary of Collective Effects Sections

We have seen that neither bunch lengthening nor the transverse mode-coupling instability will impose a significant limitation on the stored bunch current. The luminosity performance of KEKB is rather affected by the couple-bunch instabilities due to the RF cavities (longitudinally) and the resistive-wall instability (transversely). Our carefully designed damped-cavity-structure helps to reduce the longitudinal growth to a manageable level. Even the most unstable mode has a growth time (60 msec) longer than the radiation damping time of 20 msec in the LER with wiggler magnets. Transversely, however, the growth time of the resistive-wall instability ($\sim$ 5 msec) is far shorter than the radiation damping time of 40 msec. The design of the fast feedback system that can deal with the remaining growth is one of the most challenging problems for KEKB.

5.4 Beam Blow-up due to Transient Ion Trapping in the Electron Ring

In any circular machines, the beam produces ions via ionization of residual gas molecules as well as through other processes. At an electron ring which stores many bunches, these positive ions are attracted towards the beam. After several turns the ions are concentrated near the beam orbit, where they can disturb the beam motion. This phenomenon, called ion trapping, has been studied for many years. One possible cure for this problem is a partial fill, i.e., to create a contiguous group of empty RF buckets

that are unoccupied by the beam, and to let the ions drift away during this gap.

It has been recently pointed out that a somewhat different process can also degrade the beam. This effect may be called transient ion trapping. With high intensity and low emittance beams, even if the ions eventually disappear in the bunch gap, they may cause a serious effect before disappearing through the following mechanism. While each bunch ionizes the residual gas, if a bunch is displaced from the design orbit, the ions left in space will also be displaced. Such ions execute off-centered oscillations in subsequent electron bunches, and act as an amplifier for electron oscillation. The purpose of this section is to present a theoretical study of this effect.

Since the vertical emittance is much smaller than the horizontal one, the effect is more serious in the vertical plane. We assume that n_b electron bunches are followed by a gap which is long enough to sweep out the ions. This bunch pattern of n_b bunches plus a gap may be repeated several times over the ring. The first bunch of each train travels in a fresh residual gas without ions.

This phenomenon is characterized by two important parameters, Θ and K. First, the phase advance of the ion oscillation between the arrival time interval of two adjacent electron bunches is

$$\Theta = \sqrt{\frac{2zNmr_eL}{AM_N\Sigma_y(\Sigma_x+\Sigma_y)}}.$$

Here,

- z,A the electrovalence and the mass number of the ion,
- L distance between bunches,
- N number of electrons per bunch,
- Σ_j $=(\sigma_{j,e}^2+\sigma_{j,i}^2)^{1/2}$ $(j=x,y)$, where $\sigma_{j,e}$ and $\sigma_{j,i}$ are the r.m.s. beam size of electrons and ions,
- m,M_N the mass of an electron and a nucleon,
- r_e classical electron radius.

The size of the ion cloud is equal to the electron beam size when it is created. It settles down to $\sim 1/\sqrt{2}$ of the electron size after a few oscillations due to non-linear smearing. In the case of the KEKB electron ring (HER), Θ for CO^+ ions, for example, is about 0.12 radian, which means that the CO^+ ions execute one cycle of oscillation during the passage of about 50 $(=2\pi/\Theta)$ electron bunches.

The ion cloud focuses the electron beam. The number of ions is proportional to the electron bunch index n (counted from the first bunch in each train). Therefore, the tune shift is proportional to n, and is given by

$$\Delta\nu_y = RKn, \qquad K=\frac{zn_ir_e\beta_y}{\gamma\Sigma_y(\Sigma_x+\Sigma_y)},$$

where

R the average radius of the ring,
β_y average beta function,
γ electron beam energy in units of rest mass,
n_i number of ions created by one electron bunch per unit length, given by $Nn_g\sigma_i$, n_g being the number density of the residual gas and σ_i the ionization cross section. In the case of CO^+, n_i will be about 100/m.

If the oscillation amplitudes of electrons and ions are small compared with $\sigma_{y,e}$, the buildup of the oscillation may be approximately described by linear theory. Let us denote the center-of-mass position of the n-th electron bunch after travelling a distance s by $y_n(s)$. Then, the mode which is unstable against ion perturbation is given by

$$y_n(s) \approx a_0 e^{i(\Theta n - ks)},$$

where k is the betatron wave number. The conjugate mode $e^{i(-\Theta n - ks)}$ is damped.

The amplitude blowup factor of the unstable mode is approximately given, in the linear regime, by

$$G \equiv \left|\frac{a_n(s)}{a_0}\right| \approx 1 + \frac{1}{\Gamma}\exp\left[\sqrt{\Gamma + (\alpha_0\Theta n)^2} - \alpha_0\Theta n\right] \qquad (\Gamma \gg 1),$$

where

$$\Gamma = K\Theta s n^2 = \sqrt{\frac{2m}{M_N}}\frac{\beta_y L^{1/2}}{\gamma}\frac{n_g\sigma_i}{\sqrt{A}}\left[\frac{r_e z N}{\Sigma_x\Sigma_y}\right]^{3/2} s n^2$$

for $\Gamma \gg 1$. The factor $\alpha_0 \approx 0.077$ approximately takes into account the non-linear smearing of the ion center-of-mass motion. (The center-of-mass of ions oscillates approximately as $\exp(-\alpha_0\theta)\cos\theta$.) The blowup is essentially described by the factor Γ. Since the ionization cross section σ_i is roughly proportional to Z (sum of the atomic numbers of the constituents of the molecule), the ion-species dependence of Γ is $\propto Zz^{3/2}/\sqrt{A}$. Therefore, heavier ions contribute more to the instability than lighter ones, if the partial pressure is the same.

The amplitude blowup factor G for the HER is plotted in Figure 5.12 as a function of the number of turns n_t for various values of the number of electron bunches n_b. The residual gas is assumed to be CO with a pressure of 10^{-9} Torr. The e-folding time of the amplitude is about 70 turns for n_b=500 ($\propto n_b^{-2}$), although the growth with respect to n_t is not exponential.

In practice, the ion phase advance Θ can have a spread for a number of reasons. This can lead to a damping effect. For example, since Θ depends on the electron beam size, it varies over the ring. In the periodic part of the arc sections of the HER, Θ modulates between 0.10 to 0.14 radian in the case of CO^+ ions, as shown in Figure 5.13.

hhh

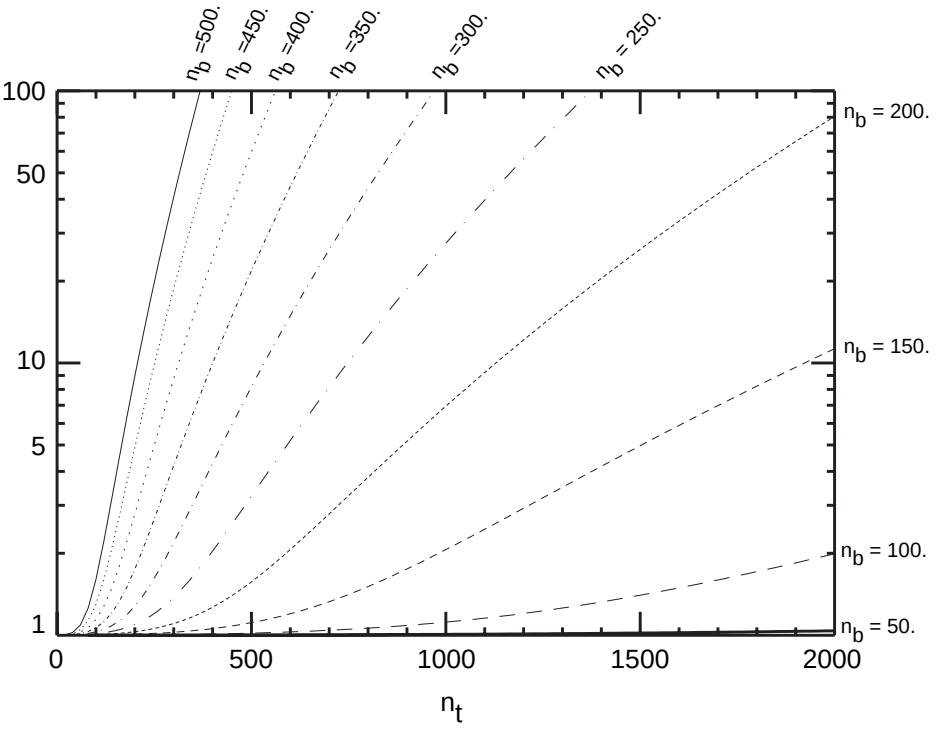

Figure 5.12: Amplitude blowup factor G for CO^+ of 10^{-9} Torr.

hhh

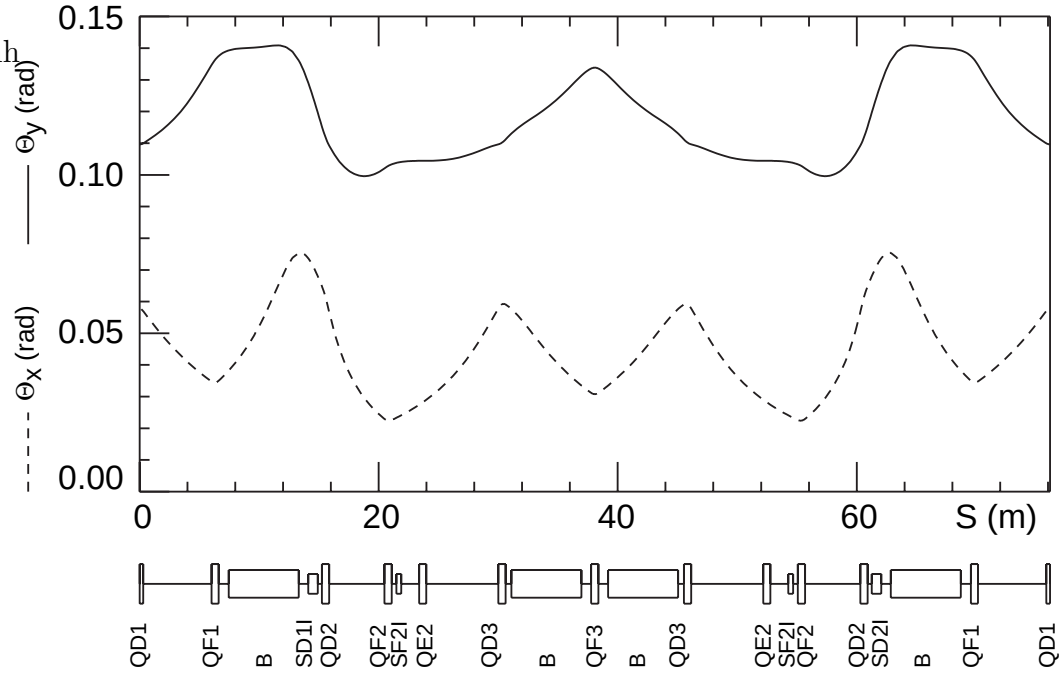

Figure 5.13: The Θ_x and Θ_y, phase advance of ion (CO^+) oscillations between the arrival of consecutive beam bunches in the HER arc.

Another reason for the spread in Θ comes from the existence of various ion species. However, since the dependence of Θ on A is weak ($\sim 1/\sqrt{A}$), the spread due to this is much smaller than the lattice effect. For example, a mixture of O_2, N_2, CO, CO_2, etc, cannot cause a more efficient spread than the lattice effect. It should be also noted that the contribution of H_2 is very small because of the small ionization cross section.

The nonlinear smearing expressed by the factor α_0 causes a similar effect. The value $\alpha_0 \approx 0.077$ has already been taken into account in Figure 5.12. It corresponds to a $\sim$30% full spread of Θ. Therefore, we cannot expect drastic damping due to the Θ spread.

Linear theory is valid only for small amplitude oscillations. It does not predict emittance growth, either. In order to take into account those effects that are ignored in linear theory, a computer simulation is being conducted. Some preliminary results are summarized here. The essential points in the simulation code are listed as follows:

1. The electron beam is represented by 10^5 macro-particles per bunch. The model ring consists only of periodic cells which are extracted in the HER arc.
2. Ions are also represented by macro-particles. Instead of a continuous distribution over the ring, they are placed at some selected points (ionization points) in the ring. It was confirmed that only a few ionization points in the ring are enough if the points are carefully selected so as to properly represent the spread of Θ. Eventually, only two points were selected for long-time calculations. The number of macro ions is at most 10^5 per ionization point. The longitudinal drift of ions is negligible.
3. The initial position of ions when they are created is that of the parent electron. The transverse velocity is generated according to the Maxwell distribution with a temperature of 300 K (this does not cause a sizable effect). Each electron bunch creates approximately 2×10^4 macro ions per point. When the number of macro ions exceeds 10^5 at one ionization point due to the passage of many bunches, some of them are randomly selected and thrown away. The subsequent ionization rate is accordingly reduced. (Although one could generate a small number of macro ions so that the final number does not exceed the limit, this is not statistically good, because the ions created by early electron bunches are more important.)
4. The interaction of an electron bunch and an ion cloud is calculated by solving the 2-dimensional (horizontal and vertical) Poison equation on a 2-D grid (64×64 to 64×256, equal space). The mesh size is typically 0.15 standard deviations in each plane. The grid for electrons and that for ions are not identical. However, because of the structure of the code, the aspect ratio (vertical to horizontal) has

to be the same. The interaction between ions is negligible.

5. The ions are assumed to disappear after interacting with n_b electron bunches before the electrons come in the next turn, so that the first electron bunch always travels in non-ionized residual gas.
6. Standard runs are performed with 512 electron bunches over 1000 turns.

The results of simulations up to now can be summarized as follows:

1. As long as the center-of-mass amplitude is small ($\lesssim$ 0.5 standard deviations), linear theory can describe the phenomena reasonably well.
2. The center-of-mass amplitude saturates at about $1\sigma_y$.
3. In order to study the effects of the bunch gaps, the electron bunch structures, like 256+[25]+256, 256+[50]+256, 128+[25]+128+[25]+128+[25]+128, etc (the number in [ ] is the number of missing bunches), have been simulated and compared with 512 continuous bunches. It turned out that the effect of up to 50 missing bunches does not considerably improve the situation.
4. The growth rate with 256 bunches (followed by long enough gap) is much smaller than that with 512 bunches as the linear theory predicts. However, the repetition of 256 bunches plus a gap of much more than 50 missing bunches will not be acceptable because of the luminosity reduction.
5. The emittance growth is about 30%.

Thus, in order to damp the growth with 512 successive bunches, a feedback system as fast as 50 to 100 turns (0.5 to 1 msec) is needed, if the gas pressure is 10^{-9} Torr. The fastest bunch mode will be about 50 bunches per cycle.

Remaining issues for future studies include:

1. It is desired to find out how many missing bunches are enough for terminating the chain of interaction. However, in order to try a longer bunch-gap, the simulation code has to be modified, because the ions after the gap extend to a large vertical dimension, whereas the newly created ions are concentrated on the axis. This ion distribution cannot be accurately expressed by an equally-spaced mesh.
2. It must be confirmed whether the emittance growth can be cured by the feedback system of the center-of-mass motion. (This is a question technically very hard to answer. The present calculation is done with a parallel processor with 64 cpu's. Interactions during tens of revolutions are simultaneously computed so that it is logically impossible to faithfully simulate a feedback system.)

5.5 Instabilities due to Beam-Photoelectron Interactions

Photoeletrons are produced by synchrotron radiation (SR) photons, when they hit the inner wall of the beam pipe. In the LER where the positrons are stored, those photoelectrons would migrate towards the beam path, where they can create a sizeable electric field. Although such individual electrons are not trapped around the beam, they form a flowing gas of electrons. Under certain conditions these photoelectrons can act as a media for transmitting perturbative forces from a particle bunch onto subsequent bunches. Thus, a coupled-bunch instability can emerge [9].

At the 2.5 GeV Photon Factory (PF) ring of KEK, when it is operated to store positrons, a coupled-bunch instability which may be consistent with this mechanism has been observed. At the PF with a stored current of 350 mA ($\sim 4\times10^9$ particles/bunch), the growth rate of the instability is much higher than the damping rate. The problem in the LER may be even more serious, since its stored current will be larger by a factor of 7.

This section presents a theoretical study of instabilities in the positron ring due to interactions between the beam and photelectrons, and discusses on a possible cure.

5.5.1 Synchrotron radiation and photoelectron

The number of photons emitted by a positron (or an electron) during one full revolution is given by[10]

$$N_\gamma = \frac{5\pi}{\sqrt{3}}\alpha\gamma \ , \tag{5.23}$$

where α and γ are the fine structure constant and the Lorentz factor, respectively. In the LER with $\gamma = 6850$, the number of photons emitted by a positron in one revolution is

$$N_\gamma = 453 \ . \tag{5.24}$$

We next estimate the production of photoelectrons by SR photons. We assume that the photoelectron production rate (quantum efficiency) is 0.02 for the copper chamber and that the energy of photoelectrons follows a Gaussian distribution with an r.m.s. value of 5 ± 15 eV[11]. Then the number of photoelectrons will be

$$N_e = 9.1/\text{particle} \ , \qquad N_{e,\text{bunch}} = N_e \times N = 3\times10^{11}/\text{bunch} \tag{5.25}$$

per revolution.

5.5.2 Coupled bunch instability caused by photoelectrons

Each photoelectron is unstable, and is lost within a short period in a presence of the positron beam due to the over-focusing effect. However, under a multi-bunch operation with uniformly filled bunches, a large number of photoelectrons are constantly supplied from the beam duct wall for every bunch passage. Consequently, the spatial distribution of photoelectrons becomes stationary. The positron bunches pass through this distribution of photoelectrons, which act as a medium of bunch-to-bunch interactions. A computer code has been developed to simulate this situation, and calculations have been carried out using the LER parameters. A full description of this method is given in [9]. A summary of the results of the calculations is presented in the following. The possible effects of magnetic fields are first ignored; cases with finite magnetic fields in the beam duct are presented later.

Figure 5.14 shows the stationary distribution of the photoelectrons. The wake force

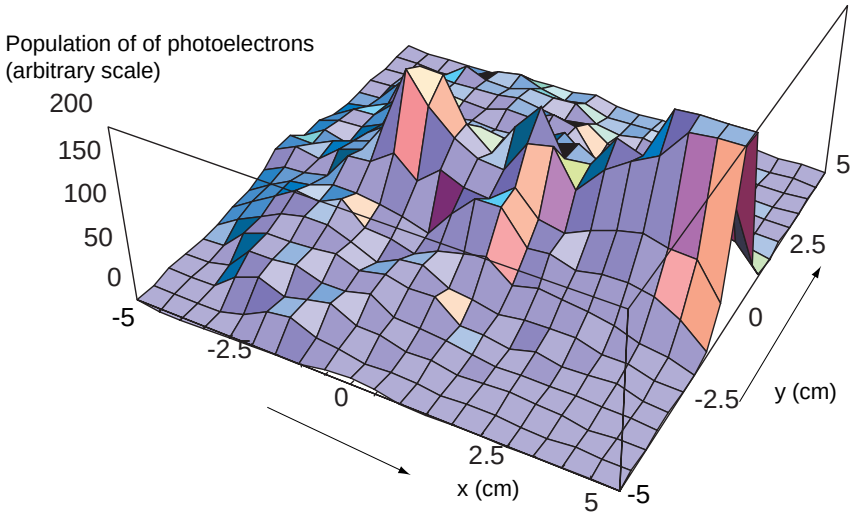

Figure 5.14: Distribution of photoelectrons in the x-y plane, where x and y refer to the horizontal and vertical coordinates (unit is cm) within the cross section of the vacuum pipe. The beam orbit is located at $(x, y) = (0, 0)$. The primary SR photons hit the inner surface of the vacuum pipe near (10, 0). Note that the LER vacuum pipe has a circular cross section an inner radius of 9.4 cm.

which causes the coupled bunch instability can be calculated by giving a perturbation to a bunch in the simulation, and by investigating the influence on the subsequent bunches. We treat the vertical instability first. Figure 5.15 shows the wake force. The wake forces are calculated in the cases of displacements of 0.5 mm and 1 mm. The linearity of the wake force can be seen. The growth rate of a coupled-bunch instability

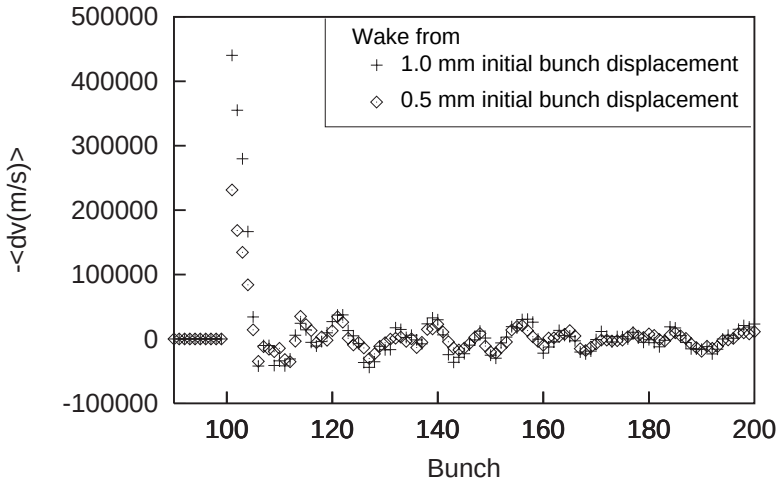

Figure 5.15: Vertical wake force. The strength of the wakes created by an initial bunch displacement of 0.5 mm (diamond and) and 1.0 mm (cross hair) are shown. It indicates that the wake strength is roughly proportional to the displacement of the initial bunch.

due to a wake force is generally given by

$$\Omega_m - \omega_\beta = \frac{1}{4\pi\gamma\nu_y}\frac{N_{e_\gamma}}{N_b}\sum_{n=1}^{n_0}\frac{d\bar{v}_y}{dy}\left(-\frac{ncT_{rev}}{h}\right)e^{2\pi i n(m+\nu_y)/h}, \tag{5.26}$$

where the mode is defined by

$$y_n^{(m)}(t) = e^{2\pi imn/h}y_0^{(m)}(t) \tag{5.27}$$

and

$$y_j^{(m)}(t) = \tilde{y}_j^{(m)}e^{-i\Omega_m t}. \tag{5.28}$$

By using the wake force found in Figure 5.15 for dv in Equation 5.26, the growth rate of the instability can be estimated. The result is shown in Figure 5.16. The maximum growth rate is found to be about 2500 s^{-1}. This is much higher than the damping rate of the LER, which is 12.8 s^{-1}. Although the head-tail damping effect will reduce the instabilities, its damping rate ($\sim$ 200 s^{-1}) will not be sufficient to cure this instability.

The horizontal wake force is shown in Figure 5.17 for bunch displacements of 0.5 mm and 1 mm. The feature of the horizontal wake force is very different from that of the vertical wake force. The linearity of the wake is broken after the passage of a dozen or so bunches. The wake force remains non-zero even after a hundred bunches. Therefore, the conventional treatment to obtain the growth rate is not applicable. (If we use this wake force in Equation 5.26, a maximum growth rate of 1700 s^{-1} is obtained). To evaluate the horizontal growth rate correctly, tracking calculations of the beam motion passing through the electron distribution will be necessary.

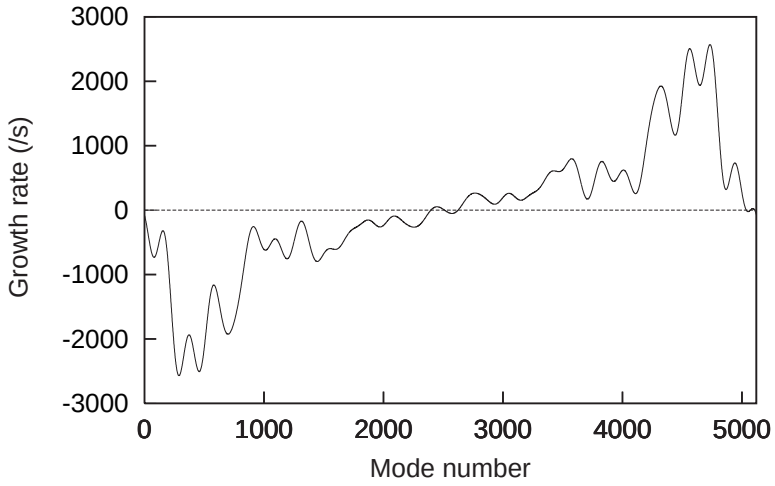

Figure 5.16: Growth rate of the vertical instability plotted against the mode number.

5.5.3 Possible cures

A possible cure for this instability is to apply magnetic fields, and to restrict the motion of photoelectrons (blocking magnetic field). For example, an electron with an energy of 10 eV has a Larmor radius of 1.1 cm in magnetic fields of 10 G. Thus the electrons will not propagate towards the beam. The wake force is expected to be smaller in this condition.

If the photoelectrons tend to reach the beam by drifting along a horizontal path, we can consider using a solenoid or a vertical dipole fields as the blocking magnetic field. Figure 5.18 shows the wake force when the solenoid field is applied in the vacuum duct with a strength of $B_z = 1$ G and 20 G. It is seen that with $B_z = 20$ G the wake force becomes small. In this condition the growth rate is estimated to be less than 200 s^{-1}.

Figure 5.19 shows the wake force when a vertical dipole field is applied in the vacuum duct. It is seen that the wake force becomes small for $B_y = 20$ G.

We next consider the case where a horizontal magnetic field is applied. Here, the electron motions are bounded on the horizontal plane. Thus, the photoelectrons produced by primary SR photons are freely allowed to reach the beam path area. Figure 5.20 shows that the wake field is stronger, as expected. The strength of the wake force shows that the wake force becomes 2.5 times larger due to the magnetic fields. By the way, we can find the cyclotron period, 18 ns, in the wake force.

Although the dominant source of photoelectrons may be concentrated on the area to be hit by primary SR photons, the effects of reflection and scattering of SR photons need to be taken into consideration. Therefore, even if the direction of the magnetic field is arranged to be vertical, electrons produced by the reflected photons may become

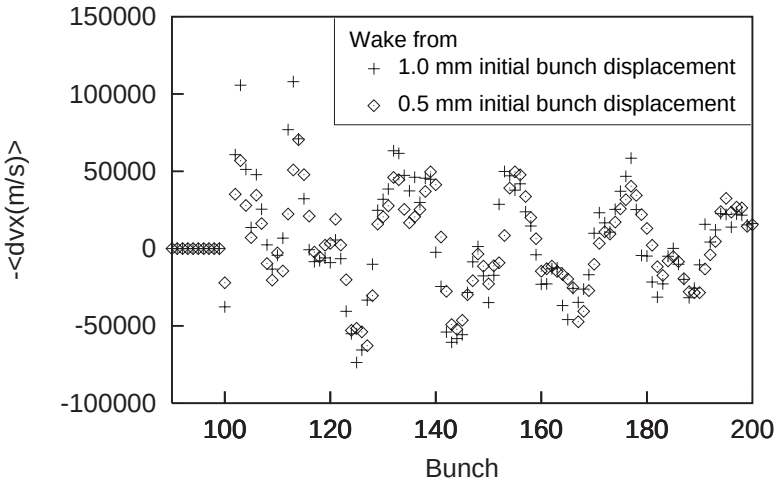

Figure 5.17: Horizontal wake force. The strength of the wakes created by an initial bunch displacement of 0.5 mm (diamond) and 1.0 mm (cross hair) are shown.

important. This has to be noted in applications to the real KEKB condition. Therefore, the use of the solenoid fields may be a better solution. By using solenoid coils of alternating field signs, the coupling effect on the beam is considered to be minimized.

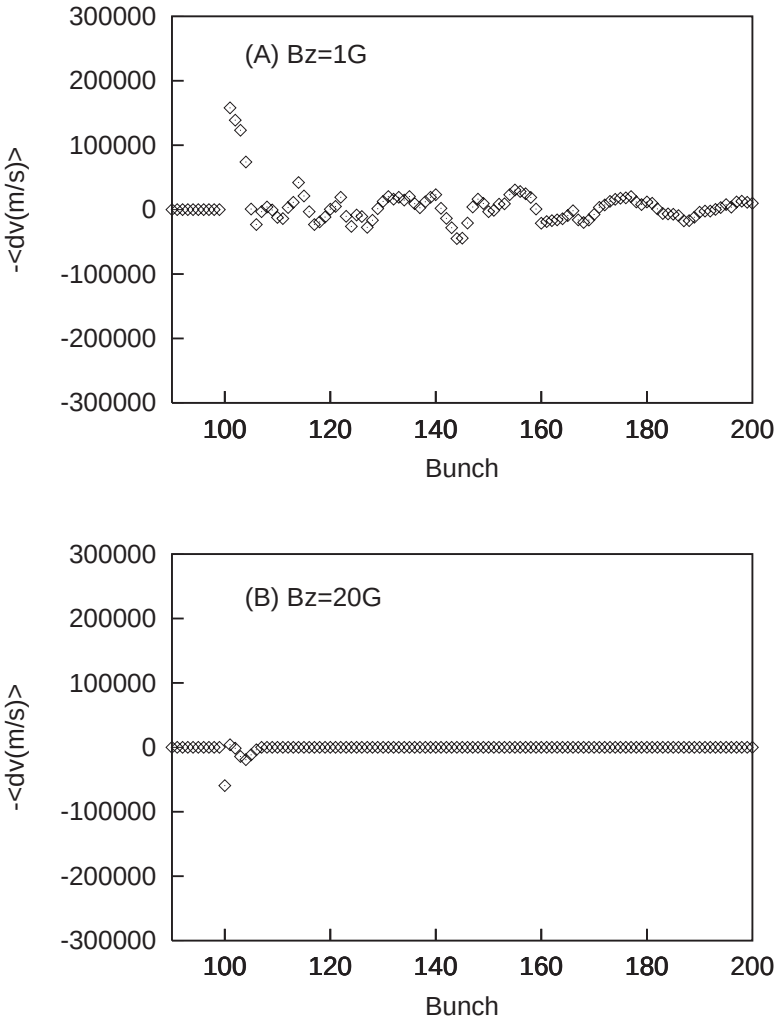

Figure 5.18: Wake force when applying solenoid fields.

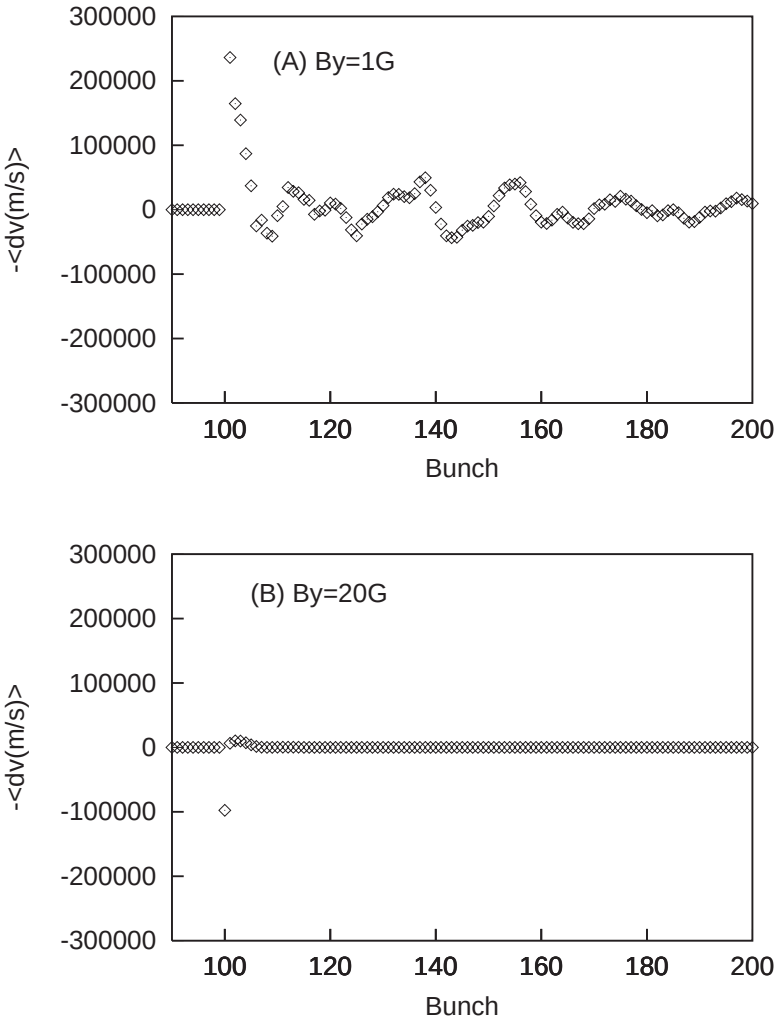

Figure 5.19: Wake force when applying vertical fields.

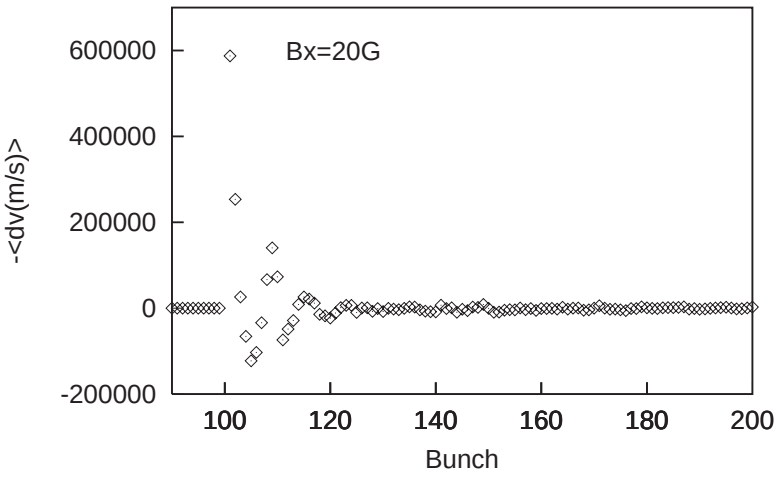

Figure 5.20: Wake force when applying horizontal fields.

5.5.4 Conclusions

The effects of interactions between the positron beam and photoelectrons have been evaluated for the LER. The growth rate is estimated to be 2500 s^{-1}. By applying solenoid or vertical magnetic fields of 20 G, the growth rate will be reduced by one order, which can be cured by the bunch-to-bunch feedback system.

Bibliography

[1] Y. H. Chin, *User's Guide for ABCI Version 8.8*, CERN SL/94-02 (AP) and LBL-35258 (1994).

[2] T. Akasaka, private communications.

[3] S. Kurennoy and Y. H. Chin, KEK Preprint 94-193 (1995). To be submitted to Part. Accelerators.

[4] R. L. Gluckstern, *Phys. Rev. A* **46**, 1106 (1992).

[5] S. S. Kurennoy, *Part. Accelerators* **39**, 1 (1992).

[6] G. V. Stupakov and S. S. Kurennoy, *Phys. Rev. E* **49**, 794 (1994).

[7] K. Oide and K. Yokoya, KEK Preprint 90-10 (1990).

[8] M. S. Zisman et. al., *Study of Collective Effects for the PEP Low-Emittance Optics*, LBL-25582 and SSRL ACD Note-59 (1988).

[9] K. Ohmi, KEK Preprint 94-198.

[10] M. Sands, *The Physics of Electron Storage Rings*, SLAC-121(1970).

[11] K. Kanazawa, private comunications.